AD NUMBER

AD864570

NEW LIMITATION CHANGE

TO

Approved for public release, distribution unlimited

FROM

Distribution authorized to U.S. Gov't. agencies and their contractors; Administrative/Operational Use; NOV 1969. Other requests shall be referred to Air Force Cambridge Research Laboratories, Attn: CRH, Hanscom AFB, MA 01730.
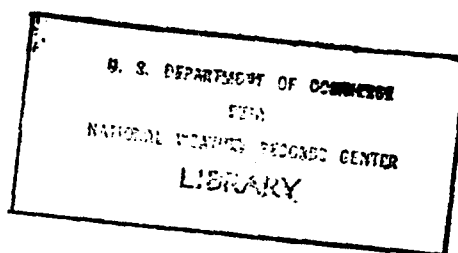
AUTHORITY

AFCRL ltr, 22 Dec 1971

AIR FORCE CAMBRIDGE RESEARCH LABORATORIES

L. G. HANSCOM FIELD, BEDFORD, MASSACHUSETTS

Interpretation and Application of Nimbus High-Resolution Infrared Radiometer Data for Southeast Asia

RUPERT S. HAWKINS

OFFICE OF AEROSPACE RESEARCH

United States Air Force

AIR FORCE CAMBRIDGE RESEARCH LABORATORIES

L. G. HANSCOM FIELD, BEDFORD, MASSACHUSETTS

Interpretation and Application of Nimbus High-Resolution Infrared Radiometer Data for Southeast Asia

RUPERT S. HAWKINS

OFFICE OF AEROSPACE RESEARCH

United States Air Force

Abstract

Comparative studies of Nimbus I and Nimbus II HRIR pictures over Southeast Asia with supporting surface and radar observations disclose that bright areas (cold temperatures) in HRIR pictures correspond to areas of precipitation revealed by radar and substantially agree with a rain index based on 12-hr rainfall reports from six stations. The Nimbus infrared pictures are significantly different from satellite daytime video pictures, however, and consequently require different interpretation.

Contents

v

Illustrations

Tables

Interpretation and Application of Nimbus
High-Resolution Infrared Radiometer Data
for Southeast Asia

1. INTRODUCTION

This paper offers an interpretation of data from the Nimbus satellite high-resolution infrared radiometer (HRIR). It has been prepared from s⁺ lies of Nimbus I (Aug through Sept 1964) and Nimbus II (May through Nov 1966) HRIR pictures over Southeast Asia compared with supporting surface and radar observations. The results will to a large degree be applicable to any satellite system operating in the 4-μ or 8- to 12-μ atmospheric windows but the ability to interpret textures and dark tones (clear or low-cloud regions), considered only briefly here, is expected to vary from one system to another. Spatial resolution and sensitivity (gray scale span) are the most important factors contributing to this variation.

The principal features of the HRIR system and pertinent characteristics of the data are only briefly described (Sec. 2) since details are available in the references. Radar and rainfall indices are compared in Sec. 3, and a number of statistical summaries of the data over Southeast Asia are discussed in Sec. 4.

2. CHARACTERISTICS OF THE NIMBUS HRIR SYSTEM AND INTERPRETATION OF THE DATA

This section briefly summarizes the HRIR system and the fundamentals necessary for a clear understanding of the following sections. One point should

be kept in mind at all times: the infrared pictures require a different inter-
pretation framework from the daytime video pictures. It should also be men-
tioned that the direct readout infrared radiometer (DRIR) system is the same as
the HRIR system. Only the method of readout is different.

2.1 The Nimbus HRIR Instrument

The HRIR system measures infrared energy in the 4-μ atmospheric window.
The instantaneous field of view is approximately 5 naut. mi. in diameter directly
below the satellite, and it varies with the angle of view. As the satellite advances
along its orbit, the system scans across the earth perpendicular to the movement
of the satellite from horizon to horizon (in tropical latitudes the scan lines are
oriented roughly east-west). The successive scans yield a strip-by-strip 'picture'
of the earth and its clouds as seen in the infrared. These HRIR pictures cover an
area over 2500 mi. wide, with the subsatellite track along its center and the
horizons along the edges of the strips. The examples given here are small sec-
tions of these strips.

Nimbus I and II were launched into sun-synchronous quasipolar orbits such
that passes occurred over the area of interest near local midday and near local
midnight. Solar reflection in the wavelength sensed by the HRIR instruments
makes daytime data very difficult to interpret. This report deals only with the
nighttime data. Operation of satellite systems in the 8- to 12-μ atmospheric
window would remove the solar reflection problem, and interpretation would then
be similar to interpretation of the nighttime data.

2.2 Basic Interpretation of HRIR Type of Data

The HRIR system measures radiant energy from the earth, clouds, and
atmosphere. For all practical purposes, however, the atmosphere is transparent
in the HRIR band. The amount of energy emitted by the earth-cloud system depends
on its temperature and emitting ability (emissivity). For all practical purposes,
the earth and relatively thick clouds emit energy equally well in the wavelength
range of the HRIR system. Emission depends on temperature: warm surfaces
emit more energy than cold ones. Since temperatures normally decrease with
altitude in the atmosphere, the earth emits more energy than clouds, low clouds
emit more energy than middle clouds, and middle clouds emit more energy than
high clouds. An exception is the high thin cloud, which allows energy to pass from
below, therefore appears warmer, and hence lower. In infrared pictures, the
warmest temperatures (land and water) register as blacks, the coldest (thick high
clouds) as whites. The grays from black to white denote temperatures from warm
to cold. The HRIR system thus provides data on cloud cover, cloud types, cloud
patterns, and cloud heights. Interpretation, however, is far from clear-cut.

One of the greatest problems is that of spatial resolution. The radiometer field of view looking straight down is a circle about 5 naut. mi. in diameter. With scattered-to-broken clouds in the field of view, the energy reaching the sensor comes from both warm earth and colder clouds. Since the resulting temperature corresponds to a level somewhere between the surface and cloud-top temperatures, a middle cloud layer could give the appearance of a low cloud layer. Besides restricting the ability to determine cloud-top height, low resolution interferes with interpretation of cloud type as well.

It must be remembered that HRIR pictures represent emitted energy around 3.7μ whereas video pictures represent reflected solar energy in the visible part of the spectrum. The greatest difference between the two systems is in the appearance of low clouds: in the infrared, low clouds are dark and often indistinguishable from land and ocean; in the video they are usually represented as light grays and whites. In some cases, the deemphasis of low clouds restricts interpretation, particularly with regard to cloud cover. In other cases—for example, when trying to locate thunderstorm areas or detect middle- and high-level vortices associated with cyclones—deemphasis of the low cloud in the HRIR significantly aids interpretation.

Details of Nimbus HRIR system can be found in Nimbus II User's Guide, 1966. Widger et al (1966) present a variety of information on the system, picture rectification, data interpretation and data application along with numerous case studies.

2.3 HRIR Interpretation in Southeast Asia

For southeast Asia the HRIR data from Nimbus II cover the period from 15 May to 20 November 1966. This includes almost all of the southwest monsoon season. The data from Nimbus I cover the short period from 30 August to 20 September 1964. Thus, by and large, the data are for the southwest monsoon season and—to repeat—for approximately local midnight. The results reported here should not be applied to other times of the day, particularly for land areas, without taking account of diurnal changes.

Comparisons of the video and infrared pictures have been made. In general, advantages of one system are disadvantages of the other, and the 12-hr separation in time adds to the problem of comparing the two. Large storm areas appear in both systems, but diurnal changes and system differences usually make it impossible to determine the rate or extent of growth or dissipation. The combination of the two systems has been useful for tracking and determining the presence of major areas of activity.
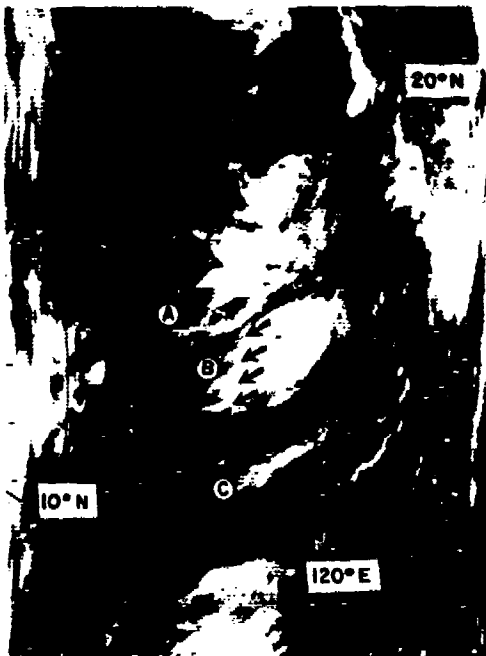
4

Figure 1. Examples of Several Types of Clouds, Including Cumulonimbi, Anvils, and Cirrus [HRIR data from Nimbus II, orbit 1522, 6 September 1966, showing (A) young convection complex, (B) several anvils merged, (C) old cirrus anvil]

The HRIR data, showing several typical features of interest, is exemplified in Figure 1. The latitude-longitude ticks mark even 2° (approx. 120 naut. mi.) intervals. The young convection complex (A) is made up of individual bright areas about 20 naut. mi. in diameter. High-level wind shear is indicated by the gradual tonal change in the anvils (B) for the large storm area marked by black arrows. The individual bright areas of the young complex do not appear to have been sheared off by the high-level winds. Either they have not reached that level or they have not been at that level very long. A thin cirrus layer spreads over the entire complex. Here, 'thin' denotes a relative transparency in the infrared. How thick and how bright these clouds would appear in the video data is not known. It is probably safe to assume that a thin cirrus layer appears semi-transparent in the infrared and in the video wavelengths as well. The very large, presumably old, anvil located at bottom center (C) is a very thin cirrus sheet several hundred miles long. Such areas of cirrus are not observed in the absence of convection complexes.

Large thunderstorms frequently appear to be made of smaller ones. This is indicated by darker tones between storms or separations between anvils near the end. The black arrows in Figure 1 indicate different thunderstorms, inferred from the separations between anvils near the end of the overall anvil. Differences

in length of the individual anvils probably reflect the relative age of the individual thunderstorms. In this case, however, the heads of the thunderstorms are not apparent in the picture.

The sharp fall-off of tone from the storms is typical. The tendency for the bright tones (cold clouds) to be elongated east-west is also typical. Some of this, if not all, is due to cirrus blowoff by the upper-level easterlies.

A tropical storm is located just off the picture, top center (122^OE, 27^ON). There are thunderstorms in the west, over Indochina. The thunderstorms in the center of the picture are located over the South China Sea. Hainan, a good geographic location for grid checking, can be seen faintly at 110^OE, 19^ON. The Gulf of Tonkin is free of clouds except perhaps low ones. Since the dark tone is solid without irregularities, the probability is that there are no low clouds. Over land this reasoning will not apply because land patterns are usually irregular.

Before quantitative measurements were made, some general conclusions were reached from comparisons of HRIR pictures and radar echo areas. About a dozen Nimbus orbits in July, August, and September 1966 were compared with radar echo areas for Ubon and Udorn in Thailand, and Saigon (Tan Son Nhut) in South Vietnam. It was found that the reported echo areas almost invariably fell within bright areas. (Bright clouds about 60 mi. southeast of Udorn gave scattered echoes at 1430 UT.) The echo areas that did not fall within bright areas were usually those comprised of scattered echoes. An example is given in Figures 2 and 3. The grid points and latitude-longitude designations are located about 1.5^O to the east and 1^O to the south of the true location. This is a gridding error. The Udorn and Saigon radar station locations are correctly marked with respect to the picture.

The grid tick spacings, 120 naut. mi., are used for judging distance from the stations. The WSR-57 at Udorn has an approximate range of 200 naut. mi. and the AN/CPS-9 at Saigon has an approximate range of 150 naut. mi. Figure 3 is a typical picture for the summer monsoon season showing a large amount of low stratiform cloud over China, thunderstorms over Indochina, and a band of storms from the Taiwan-Philippine region across the South China Sea and lower Indochina.

In defining terms for comparing bright areas (and therefore cold temperatures) with radar echo areas and surface reports, and definite tone contrast with other tones, bright areas are denoted 'dense high cloud' (DHC) to differentiate them from high cloud in general.

The tendency is for DHC to occur in discrete subdivisions of larger cloud areas commonly referred to as 'blobs' or 'clusters.' A tally of these areas was made for 24 orbits in the area bounded by 100° to 110^OE and 10° to 20^ON, the 10° block that encompasses most of Indochina. To allow quick and easy estimation of the size of DHC areas from the 2^O grid ticks on the pictures, squares
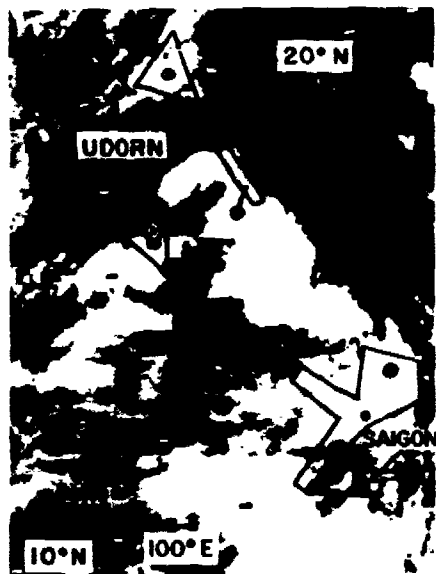
6

Figure 2. Radar Echo Areas Superposed on the
HRIR Data for Stations Udorn and Saigon (Nimbus II,
orbit 777, 12 July 1966, 1650 UT; time of radar is
1530 UT, 2330 local time)

Figure 3. The Same HRIR Data as in Figure 2
but for a Larger Area and Without Radar Echo Areas
(The dashed line marks Indochina.)

having lengths of 0.25°, 0.5°, 1°, 2°, 3°, and 4° latitude on a side were chosen.
The areas correspond of course to the square of the respective side.

Merged storms attached laterally by more than half the length of the smaller
storm were counted as one storm; otherwise, as two storms. The storm in the
center of Figure 1 falls into the 3° category. The storm about 5 naut. mi. ESE of
Udorn in Figure 2 falls into the 1° category. The mean frequency per day of the
storm count derived from 24 orbits is given in Figure 4. Also shown are the cor-
responding frequencies of the mean storm areas per day. The total area of the
1° and 2° size storms (6.7 deg^2) is about twice as large as the areas of all the
other sizes combined (3.5 deg^2).

Figure 5 shows a frequency distribution of the daily amount of DHC (in tenths)
over the area of SEA bounded by 100° to 110°E and 10° to 20°N. This 10° box in-
cluded 0.40 coverage or more of DHC only 6 percent of the time, the mean coverage
being about 0.15. This figure reiterates the earlier statement concerning the
special nature of DHC, namely, that it is considerably restricted by comparison
with cloud coverage in general. Comparisons with radar and rainfall data presented
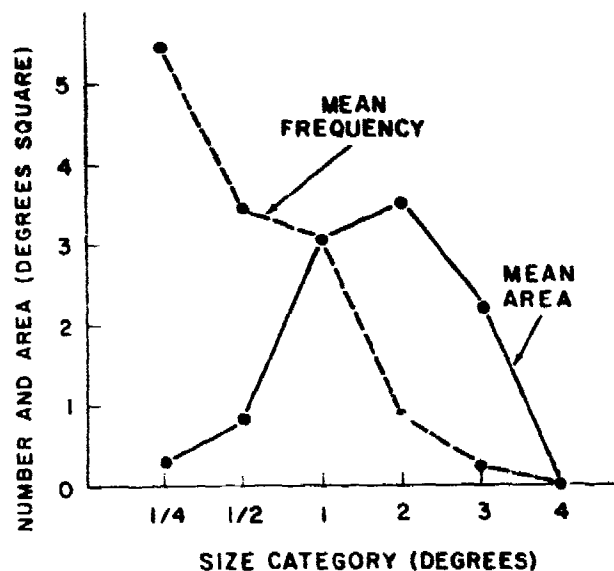in the next section will further emphasize this point.

Figure 4. Mean Frequency and Mean Area of Coverage for
Various Categories of Thunderstorm Areas, 100° to 110°E
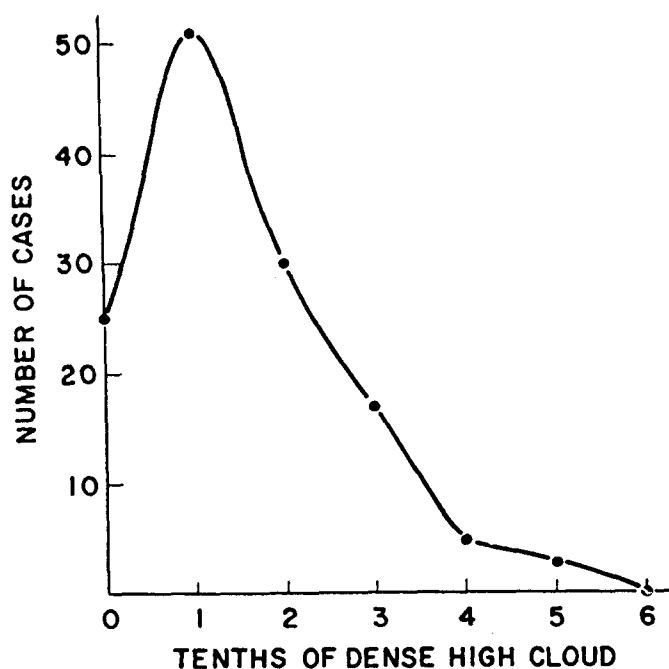and 10° to 20°N (24 cases, 15 May to 1 July 1966)

Figure 5. Frequency Distribution of Coverage of Bright
Area Defined by 100° to 110°E and 10° to 20°N (131 cases,
15 March to 1 November 1966)

3. DENSE HIGH CLOUD VERSUS RADAR AND RAIN INDICES

Comparisons of radar echo areas with DHC indicate a relationship between
rain areas and DHC areas. This and the fact that DHC coverage comprises about
one-fourth of the clouds over Indochina prompted a quantitative analysis. Saigon
radar data were used to obtain radar indices for a circle of 50 naut. mi. radius
(see Fig. 6). Echo areas were weighted (0.25, scattered; 0.70, broken; 0.95,
solid; and 1.00, 'cell') to obtain an estimate of the rain area deduced from the
radar echo areas. The Radar Index (RI) is this area divided by the total area in
the 50 naut. mi. circle. The DHC readings, in units of 10 percent of coverage,
were made for squares 2° latitude by 2° longitude, one centered at Saigon and
four overlapping the center square such that their adjacent corners meet at the
center of the central square (Figure 6). The mean percentages of DHC coverage
for 53 cases in June, July, and August 1966 for the five boxes are as follows
(for geographic regions, see Figure 6):

Except for the Delta box (lower left), the averages for land show almost 10 percent more coverage (40 percent more DHC) than the ocean box (lower right). The Saigon box is closer to the inland averages than to the ocean value. A correlation coefficient of 0.70 was obtained between DHC in the central box and the RI.

To reduce random reading errors, an independent reading of DHC was made. Alone, it gave the same coefficient; and the average of the two readings gave a correlation coefficient of 0.79. The data are plotted in Figure 7 together with the least-squares line of best fit.

Some estimates of the probability of rain occurring at a point in DHC can be made. When DHC is 100 percent, the regression equation gives an RI of 50.4. This may be representative of large areas of thunderstorms but is too high for DHC as a whole. If rain occurred only in DHC, the mean percent area would be 47.4, which is the mean RI divided by the mean DHC. As can be seen from Figure 7, rain occurs in some cases where DHC is zero percent. The 14 cases where DHC is zero percent give an average RI of 1.6. Assuming that this value is representative of the entire area without DHC,

$$1.6(1-\overline{DHC}) + F(\overline{DHC}) = \overline{RI} , \tag{1}$$

where $\overline{DHC}$ = mean DHC cover, F = percent of rain area in $\overline{DHC}$, and $\overline{RI}$ = mean RI. Solving for F,

$$F = \frac{\overline{RI} - 1.6(1-\overline{DHC})}{\overline{DHC}}$$

$$= \frac{10.9 - 1.6(1-0.23)}{0.23}$$

$$= 42.0 \text{ percent .}$$
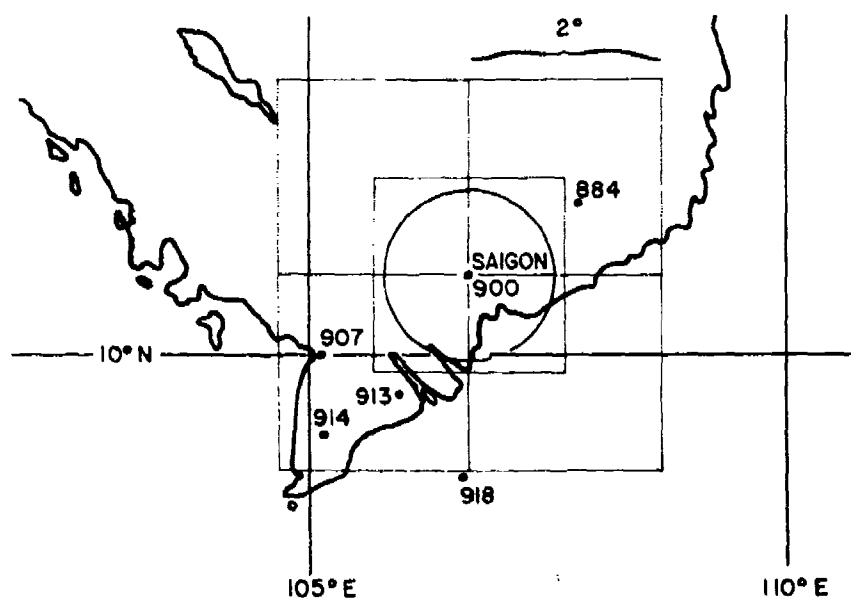
Figure 6. Base Map for Comparisons of Dense High Cloud With Radar and Rain Indices (The boxes are 2° latitude by 2° longitude, and the circle has a 50-naut. mi. radius. The six stations used for the precipitation index are 884, 900, 907, 913, 914, and 918.)
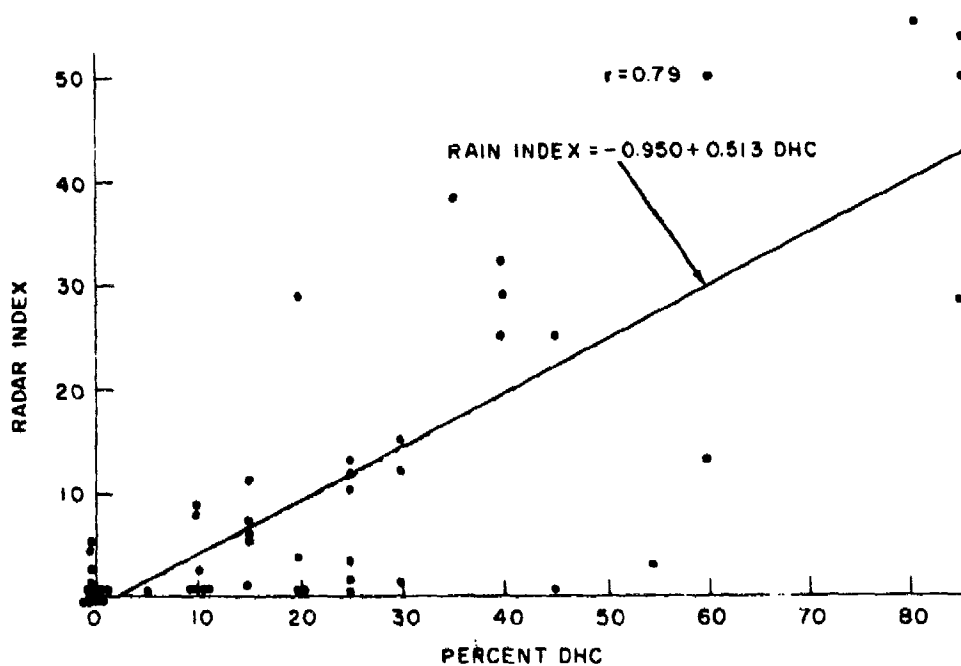

Figure 7. Dense High Cloud Percentage Versus Radar Index and Line of Regression (53 cases; June through August 1966; Saigon)

Assuming that rain is equally likely at all points in the 50-naut. mi. circle around Saigon, the RI is the probability of rain occurring at a point in the area. For the cases under discussion the value of the mean RI is 10.9 percent, about one-fourth as large as F, which points up the value of knowing whether or not DHC is present.

Another interesting comparison can be made with F. The total cloud coverage reported by meteorologic stations is not known for the area and cases under discussion. The climatologic mean, however, is known to be about 80 percent for June, July, and August at Saigon.* In the following discussion, values for 75 percent and 85 percent appear in parentheses after the value for 80 percent coverage. As in Eq. (1), we write,

$$0(1-C) + G'C = \overline{RI},$$

where C is the cloud coverage and G is the percentage of rain area in the cloud. Solving for G,

$$G = \frac{\overline{RI} - 0}{C}$$

$$= \frac{10.9}{0.80 \ (0.75, 0.85)}$$

$$= 13.6 \text{ percent } (14.5 \text{ percent, } 12.8 \text{ percent}),$$

which is about one-third as large as F.

The HRIR observations were made almost in the middle of a 12-hr accumulated precipitation observation. Since precipitation is widely variable in time and space, an arbitrary 12-hr rainfall index based on the six stations shown in Figure 6 was devised, with a scale from 0 to 9 as defined in Table 1. A correlation coefficient of 0.65 was obtained for DHC and the rain index. The data points and regression line are given in Figure 8. More frequent satellite measurements would undoubtedly refine the relationship.

The HRIR results indicate that bright areas (Dense High Cloud) are areas of deep cumulus convection. This represents an important advantage over the video system since video pictures lack the ability of HRIR pictures to accentuate the difference between bright low stratiform clouds and bright deep cumulus convection.

---

* The 34-yr record Climate of Republic of Vietnam, 20th Weather Squadron, 1st Wea Wg (MATS), p. 94, gives mean cloudiness of 78 percent for June, 82 percent for July, and 79 percent for August.

Table 1. Six-Station Rain Index

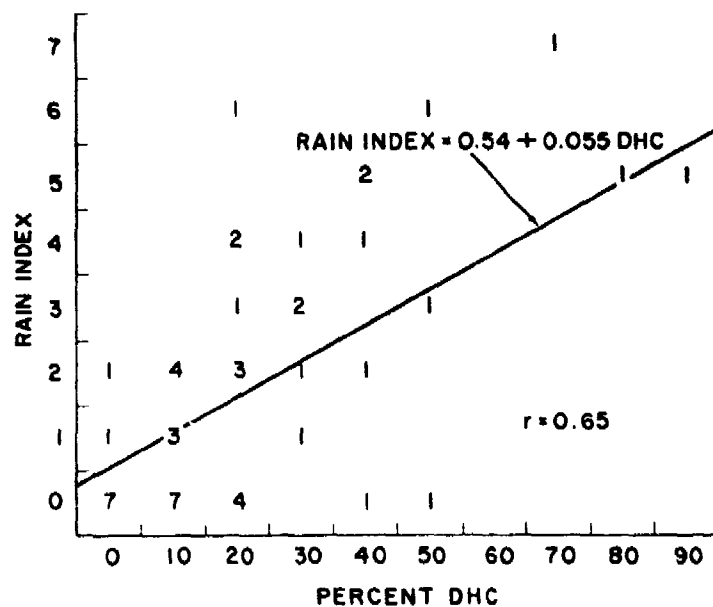| Stations Recording < 5 mm	Millimeters of Precipitation at Station Recording Largest Value				
	< 5	≥5 < 10	≥10 < 20	≥20 < 50	≥50
6	0	-	-	-	-
5	-	1	2	3	4
4	-	2	3	4	5
3	-	3	4	5	6
2	-	4	5	6	7
1	-	5	6	7	8
0	-	6	7	8	9

Figure 8. Dense High Cloud Percentage Versus Rain Index
and Line of Regression (53 cases; June through August
1966; 12-hr rain index, six stations)

I. SOME DENSE HIGH CLOUD SUMMARIES

To get some idea of the small-scale geographic distribution and large-scale day-to-day variations in DHC, analyses were performed as detailed below.

1.1 Small-Scale Monthly Means

The relationships found between DHC and the precipitation indices in the previous section led to making 1^O readings of DHC percentage for June, July, and August 1966 (24 days in June, 14 in July, and 19 in August). The monthly means are presented in Figure 9.

In June 1966 the South China Sea was very inactive. Ocean areas in this region generally do tend to be inactive, and land areas active, in June. An exception shows in the top left corner of the chart (Figure 9). The Burma area is low, and the northern part of the Bay of Bengal is high in DHC coverage. The same tends to hold true for July except that coverage over the South China Sea has gone up, with an active center located at about 11^ON, 114^OE. This active area is also present in August at 13^ON, 116^OE. Activity over Indochina is high in August, compared with June and July.

1.2 Large-Scale Day-to-Day Variations

Large-scale day-to-day variations were investigated by examining the percent coverage of dense high cloud over SEA between latitudes 10° to 20^ON and longitudes 100° to 110^OE, as shown in Figure 10. These readings indicate a tendency toward 'pulses' of a week to ten days long.

The statistics on 24-hr change in DHC coverage from 15 May to 1 November 1966 for the SEA area (100° to 110^OE, 10° to 20^ON) are summarized in Figure 11. The number of cases of various amounts of DHC 24 hr after a given amount of DHC is plotted in Figure 11(a). For instance, 2/10 DHC was followed by 1/10 DHC 14 times and by 0/10 DHC zero times; 3/10 DHC was followed by 3/10 DHC 5 times. Figure 11 (b) shows how the distribution would look if no connection (random) between consecutive nights is derived from the frequency distribution of DHC (Figure 5). Figure 11 (c) shows the excess (or deficit) of cases observed over what would be expected if the amounts of DHC occurred at random. For example, there is a tendency for 2/10 DHC to decrease to 1/10 DHC but not to 0/10 DHC. Zero-tenths is very persistent.

The best forecast based on the observations given in Figure 11 (a) and for a minimized rms error is given in Figure 12, together with the persistence forecast. The abcissa and ordinate are in tenths of coverage. The greatest difference is on the high end, where it is about one-tenth at four-tenths coverage.
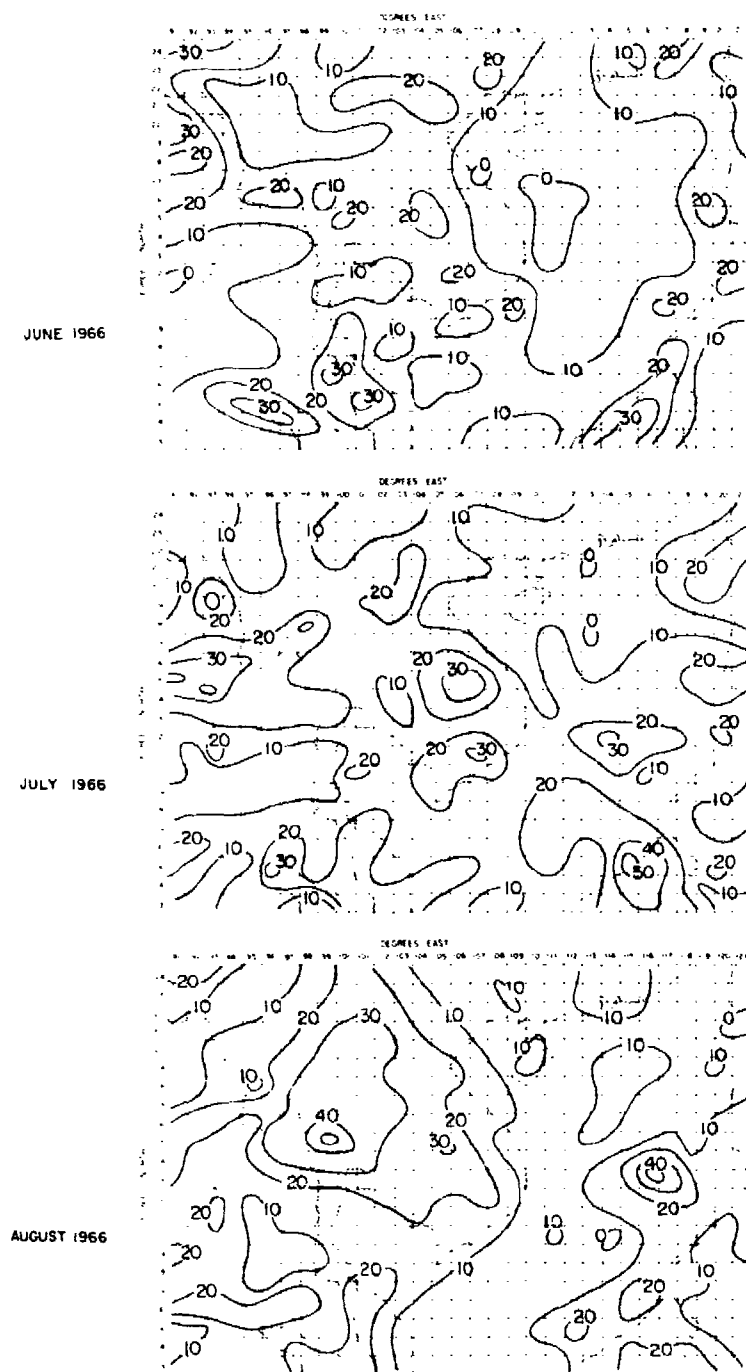
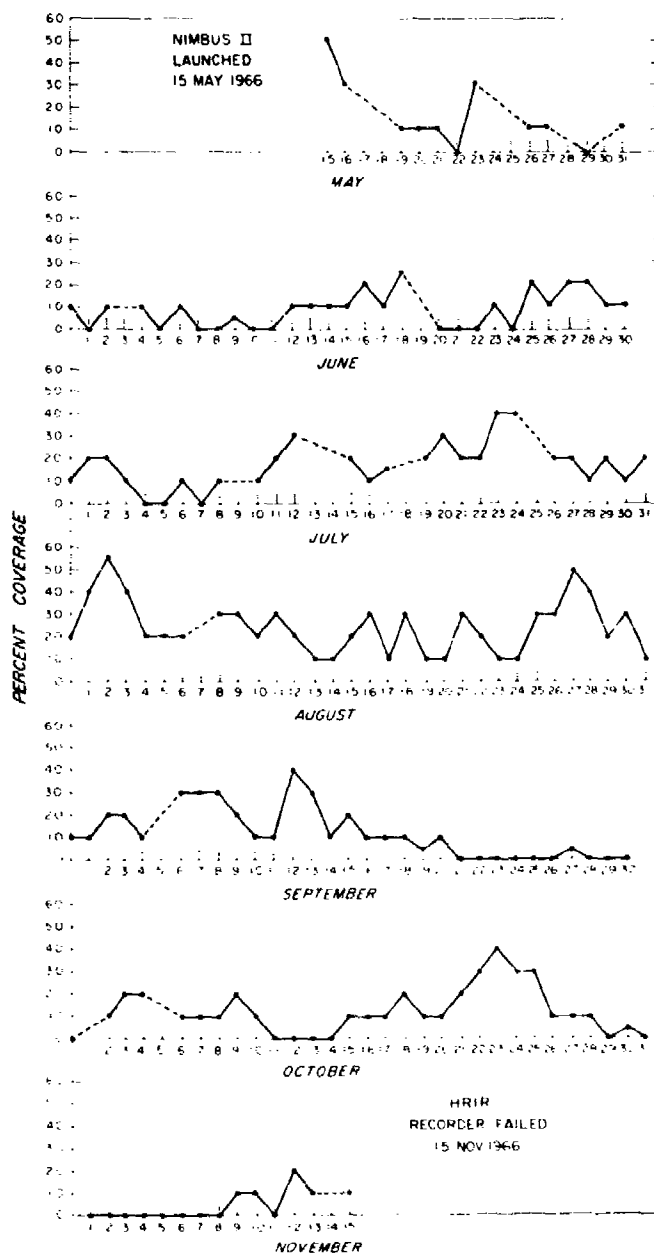Figure 9. Mean Percent of Dense High Cloud, 1° Squares, for June, July, and August 1966

Figure 10. Percent of Dense High Cloud for the Area Over
Indochina Bounded by 10° to 20°N and 100° to 110°E
(15 May to 15 November 1966)

(a)

(b)

(c)

Figure 11. Summary of 24-hr Changes in DHC for the Area Over Indochina
Bounded by 10° to 20°N and 100° to 110°E [(a) distribution observed, (b) random
distribution, (c) observed minus random distribution]
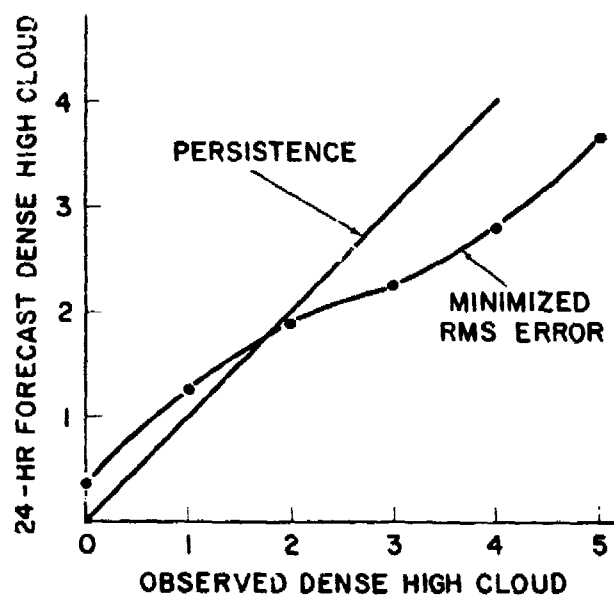
Figure 12. Persistence and Minimized RMS Error Forecast for 24 hr for DHC in Area Over Indochina Bounded by 10° to 20°N and 100° to 110°E
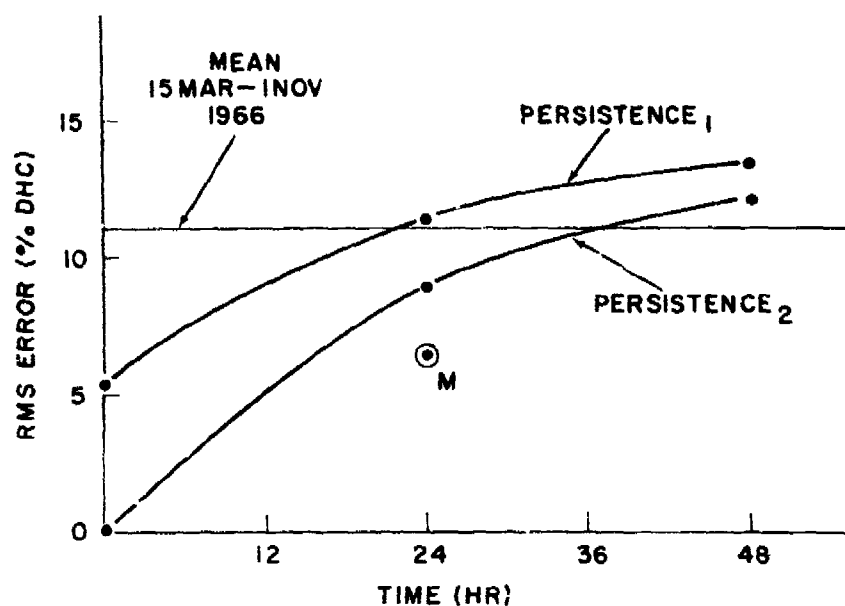

Figure 13. Persistence₁ (With Reading Error), Persistence₂ (Without Reading Error), and Mean DHC Versus Time

Figure 13 gives the error (percent DHC) with time for the seasonal mean forecast for readings with random errors (persistence$_1$) and for readings without random reading errors (persistence$_2$). It will be noted that the 24-hr rms error for persistence$_1$ is about equal to the error for the climatologic mean. The point M is for the minimized rms prediction without reading error. The reading error is based on results of three readings of two hundred 10° by 10° boxes. These results are of course for midnight readings. For other times, diurnal changes should be taken into account.

These results indicate that there are large-scale slow-moving or varying systems producing areas of activity. The same impression is given by video and infrared pictures of 'blobs' and long broad bands of activity but studies of synoptic maps in conjunction with satellite pictures have not revealed any definitive relationships.

5. CONCLUSIONS

Nighttime HRIR pictures are significantly different from the satellite video pictures, and therefore require different interpretation. Bright tones (DHC) substantially agree with radar and rainfall indices. Over Indochina there is some persistence of DHC from one day to the next.

Acknowledgments

I wish to thank my coworkers of the Satellite Meteorology Branch for their numerous suggestions.

References

Staff Members, NASA (1966), Nimbus II Users' Guide, Washington, D.C.

Widger, W.K., et al (1966), Meteorological Interpretation of Nimbus High-Resolution Infrared (HRIR) Data, NASA Contractor Report CR-312, Washington, D.C.

DOCUMENT CONTROL DATA - R&D

(Security classification of title, body of abstract and indexing annotation must be entered when the overall report is classified)

1. ORIGINATING ACTIVITY *(Corporate author)*	2a. REPORT SECURITY CLASSIFICATION
Air Force Cambridge Research Laboratories (CRH) L.G. Hanscom Field Bedford, Massachusetts 01730	UNCLASSIFIED 2b. GROUP

3. REPORT TITLE

INTERPRETATION AND APPLICATION OF NIMBUS HIGH-RESOLUTION INFRARED RADIOMETER DATA FOR SOUTHEAST ASIA

4. DESCRIPTIVE NOTES *(Type of report and inclusive dates)*

Scientific.   Interim.

5. AUTHOR(S) *(First name, middle initial, last name)*

Rupert S. Hawkins

6. REPORT DATE	7a. TOTAL NO. OF PAGES	7b. NO. OF REFS
November 1969	25	2

8a. CONTRACT OR GRANT NO.	9a. ORIGINATOR'S REPORT NUMBER(S)
b. PROJECT, TASK, WORK UNIT NOS. 6698-03-01	AFCRL-69-0485
c. DOD ELEMENT 62101F	9b. OTHER REPORT NO(S) *(Any other numbers that may be assigned this report)*
d. DOD SUBELEMENT 681000	ERP, No. 308

10. DISTRIBUTION STATEMENT

2—This document is subject to special export controls and each transmittal to foreign governments or foreign nationals may be made only with prior approval of AFCRL (CRH).

11. SUPPLEMENTARY NOTES	12. SPONSORING MILITARY ACTIVITY
TECH, OTHER	Air Force Cambridge Research Laboratories (CRH) L.G. Hanscom Field Bedford, Massachusetts 01730

13. ABSTRACT

Comparative studies of Nimbus I and Nimbus II HRIR pictures over Southeast Asia with supporting surface and radar observations disclose that bright areas (cold temperatures) in HRIR pictures correspond to areas of precipitation revealed by radar and substantially agree with a rain index based on 12-hr rainfall reports from six stations. The Nimbus infrared pictures are significantly different from satellite daytime video pictures, however, and consequently require different interpretation.

DD FORM 1473 (1 NOV 65)

14. KEY WORDS	LINK A		LINK B		LINK C	
	ROLE	WT	ROLE	WT	ROLE	WT
Satellite meteorology HRIR data Nimbus satellites Southeast Asia						